Observation of Oscillatory Surface Reactions of Riboflavin, Trolox, and Singlet Oxygen Using Single Carbon Nanotube Fluorescence Spectroscopy

Fatih Sen,[†,‡,#] Ardemis A. Boghossian,[†,#] Selda Sen,[†,‡] Zachary W. Ulissi,[†] Jingqing Zhang,[†] and Michael S. Strano[†,*]

[†]Department of Chemical Engineering, Massachusetts Institute of Technology, 77 Massachusetts Avenue, Cambridge, Massachusetts 02139, United States and [‡]Department of Chemistry, Middle East Technical University, 06531 Ankara, Turkey. [#]These authors equally contributed to this work.

ABSTRACT Single-molecule fluorescent microscopy allows semiconducting single-walled carbon nanotubes (SWCNTs) to detect the adsorption and desorption of single adsorbate molecules as a stochastic modulation of emission intensity. In this study, we identify and assign the signature of the complex decomposition and reaction pathways of riboflavin in the presence of the free radical scavenger Trolox using DNA-wrapped SWCNT sensors dispersed onto an aminopropyltriethoxysilane (APTES) coated surface. SWCNT emission is quenched by riboflavin-induced reactive oxygen species (ROS), but increases upon the adsorption of Trolox, which functions as a reductive brightening agent. Riboflavin has two parallel reaction pathways, a Trolox oxidizer and a photosensitizer for singlet oxygen and superoxide generation. The resulting reaction network can be detected in real time in the vicinity of a single SWCNT and can be completely described using elementary reactions and kinetic rate constants measured independently. The reaction mechanism results in an oscillatory fluorescence response from each SWCNT, allowing for the simultaneous detection of multiple reactants. A series-parallel kinetic model is shown to describe the critical points of these oscillations, with partition coefficients on the order of 10^{-6}—10^{-4} for the reactive oxygen and excited state species. These results highlight the potential for SWCNTs to characterize complex reaction networks at the nanometer scale.

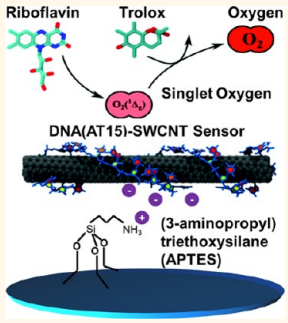

KEYWORDS: single-walled carbon nanotube (SWCNT) · fluorescence · sensor · deoxyribonucleic acid · (DNA AT15) · single molecule · Trolox · riboflavin · singlet oxygen · triplet state · scavenging (scavenger)

Riboflavin, or vitamin B2, is an essential micronutrient that plays a key role in regulatory health functions[1−4] such as body growth and development,[5−8] red blood cell formation,[8,9] hormone production and regulation,[9] and sensitization of tumor cells for apoptosis.[10] Riboflavin also plays an important role in the production of metabolic energy in the electron-transfer system by metabolizing carbohydrates, lipids, and proteins.[11−14] Owing to its omnipresent availability in frequently consumed goods such as milk, yeast, vegetables, and beer, riboflavin has been extensively studied as a photosensitizer in food[14−19] and biological systems.[20,21] Under illumination with visible or UV light, riboflavin is excited to the singlet state (^{1}RF*), which then relaxes to the triplet excited state (^{3}RF*).[22] The ^{3}RF* reacts with oxygen either directly in a type-II pathway to form singlet oxygen or *via* hydrogen or electron transfer in a type-I pathway to form free radicals.[11,23] The presence of singlet oxygen and radical products formed from the type-I and type-II reaction pathways results in subsequent riboflavin instability and degradation.[24−26]

To address issues of instability, such photosensitizers are often coupled with naturally occurring tocopherols and vitamin E-type compounds that demonstrate antioxidant behavior.[27] The addition of one such tocopherol, Trolox, has been shown to prolong the shelf life of riboflavin-containing food products such as milk[28] and soybean oil[29] *via* effective reactive oxygen species (ROS) scavenging. The reactive intermediates in the Trolox−riboflavin oxidative system of reactions have been measured in bulk using a combination of oxygen electrodes, as well as flash and static photolysis measurements, and the systems of reactions have been

* Address correspondence to strano@mit.edu.

Received for review August 15, 2012 and accepted October 17, 2012.

Published online October 18, 2012
10.1021/nn303716n

modeled previously.[25] However, the simultaneous, single-molecule measurement of such a heterogeneous system of reactive species remains unseen.

In previous studies, single-molecule measurements of ROS were achieved using single-walled carbon nanotubes (SWCNTs) as near-infrared fluorescent detectors of such species.[30−33] SWCNTs possess several advantages as sensors, including sensitivities that extend to single-molecule interactions.[34−40] To promote monodispersion in aqueous environments, SWCNTs are suspended in a variety of polymeric and surfactant-based wrappings[41−43] that can impart selectivity toward a specific analyte. The surrounding SWCNT environment, which may induce charge transfer or undergo conformational changes in the presence of an analyte, imparts the nanotube with an optical sensing mechanism. Such a mechanism has been used in the development of sensors selective for glucose,[44−46] DNA polymorphism and hybridization,[47,48] ATP,[49] and nitric oxide (NO).[50] This approach has been extended to detect analytes down to the single-molecule level, where individual molecular binding events result in the stochastic fluctuation of a nanotube's fluorescence.[32,51] Understanding how to discern the reaction pathways of an unstable analyte using SWCNT emission can extend this detection platform to more complex molecules and collections of molecules.

In this study, we identify, for the first time, the signature of the complex decomposition and reaction pathways of riboflavin using isolated SWCNT sensors dispersed onto a (3-aminopropyl) triethoxysilane (APTES) coated glass slide. The SWCNT emission is quenched by riboflavin-generated ROS, but increased by Trolox, which has been shown by Krauss and co-workers to function as a reductive brightening agent.[52] Because riboflavin oxidizes the Trolox and is also a photosensitizer for $^1O_2$ generation, the disparity in the rates for each of these reactions creates an oscillatory fluorescence response from each isolated SWCNT or bundle on the surface. The oscillations provide an opportunity to analyze these complex reaction pathways that are otherwise difficult to study at the surface of a single nanoparticle. The detection of multiple species using SWCNT emission was previously demonstrated by our laboratory as an example of multimodality.[53] However, this work demonstrates this method for a reactive system. A series-parallel kinetic model is shown to describe the critical points of these oscillations, allowing for parameter estimates of the corresponding partition coefficients of the reactive species.

RESULTS

Figures 1a and 1b show the experimental setup used to measure and compare riboflavin quenching of a fluorescent film of SWCNTs adsorbed to a microscope slide in the presence and absence of the reducing brightening agent, Trolox. The incubation and absorption are conducted such that approximately 200−300 diffraction limited fluorescent spots are visible for analysis. Frequency distribution histograms compare the starting and ending fluorescence intensities of the individual SWCNTs in the presence of oxygen for (c) just riboflavin addition, (d) riboflavin addition before Trolox incubation, (e) Trolox addition before riboflavin incubation, and (f) riboflavin and Trolox addition at the same time. Upon riboflavin addition to the SWCNT sensors, the fluorescence emission is quenched (Figure 1c). If Trolox is added after riboflavin incubation, the amount of quenching is less pronounced (Figure 1d) compared to the case in the absence of Trolox (Figure 1c). This decrease in the riboflavin quenching response in the presence of Trolox is attributed to the contrasting, brightening effect of Trolox that has been observed in previous studies.[52] If Trolox is added prior to riboflavin addition (Figure 1e), or Trolox and riboflavin are added simultaneously (Figure 1f), the degree of total SWCNT quenching is less pronounced than that observed in the previous cases. In all cases, the starting intensity distribution (red) is skewed toward dimmer SWCNTs. This initial distribution is an artifact of the SWCNT-selection algorithm used in this study, which selects nanotubes based on their brightness within the first frame of the movie. The algorithm first selects the brightest nanotubes, then the next brightest nanotubes, and so on, until the 200 brightest, most sensitive nanotubes are selected. After analyte addition, the final intensity distribution (blue) becomes more Gaussian, indicative of the nonlinear effects analyte addition has on SWCNTs that vary in length, chirality, sensitivity, number of defects, reactivity, etc.

A birth-and-death Markov model was used to extract concentration-dependent apparent rates based on stochastic fluctuations in nanotube fluorescence due to single-molecule binding events. A detailed description of the model can be found in our previous work.[31,54,55] To summarize, the algorithm consists of three analytical steps: (1) extraction of fluorescence versus time traces from individual SWCNTs or collections of nanotubes which appear as diffraction-limited spots, (2) fitting of these experimental traces to idealized, de-noised, multi-step functions to identify transitions from noise, and (3) calculation of the rate constant from the event information.

In the first step, which is the extraction of traces from individual SWCNTs, experimental fluorescence *versus* time data were collected using a Zeiss AxioVision inverted microscope with 658 nm laser excitation coupled to a 2D InGaAs imaging array (Figure 1a). Petri dishes containing DNA-wrapped films (Figure 1b) in the presence of 2 mL of argon-bubbled phosphate buffer saline (PBS) were placed on the microscope, and a series of consecutive movie images of the fluorescing

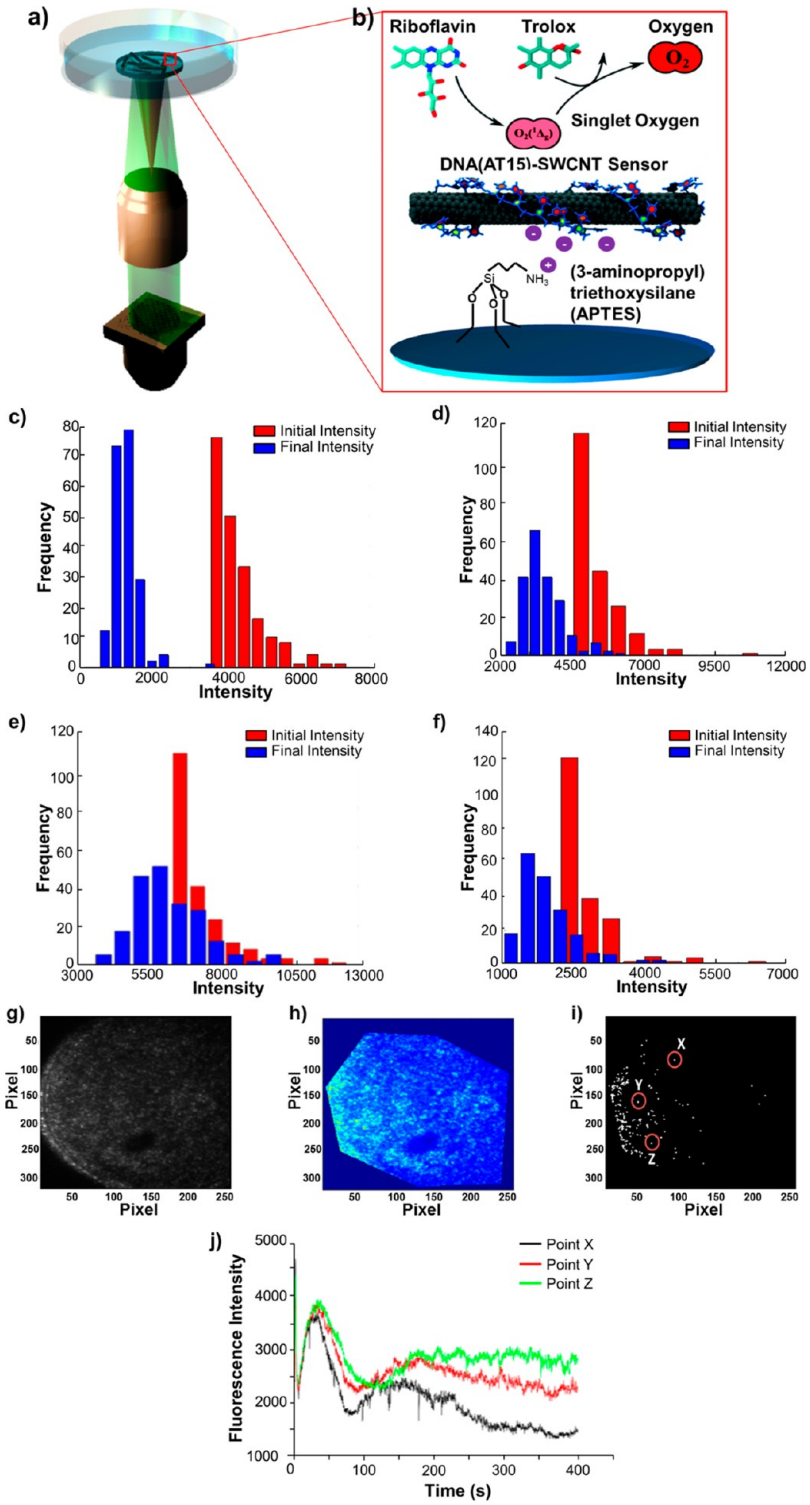

Figure 1. Fluorescent SWCNT array capable of detecting singlet oxygen. (a) Schematic of the microscope setup. A 658 nm laser beam (red) excites at the SWCNT array deposited on the glass-bottomed Petri dish. The emission light (green) is collected by a near-infrared array detector through a 100× TIRF objective mounted on an inverted microscope. The laser power at the sample is 33.8 mW. (b) Sample configuration of the SWCNT array: individual AT_{15}-SWCNT complexes are deposited on the Petri dish, which is pretreated by APTES, through electrostatic interactions. (c–f) Histograms showing frequency distributions of starting and ending intensities of individual SWCNTs in the presence of oxygen for (c) just riboflavin addition, (d) Trolox addition after riboflavin incubation, (e) riboflavin addition after Trolox incubation, and (f) riboflavin and Trolox addition at the same time. (g–i) Fluorescence images of DNA-wrapped SWCNT films: (g) sample image of the first frame of a movie, where the bright spots are the fluorescence emissions from individual SWCNTs. Pixel intensities were averaged over 2 × 2 pixelated regions, typical of diffraction-limited SWCNT emissions; h) cropped image from panel g, where SWCNTs located near the outer ring of the laser boundary are removed; (i) image representing the location of the 200 brightest nanotubes that were selected within the cropped image in panel h. (j) Representative intensity–time traces for selected individual SWCNTs in image i.

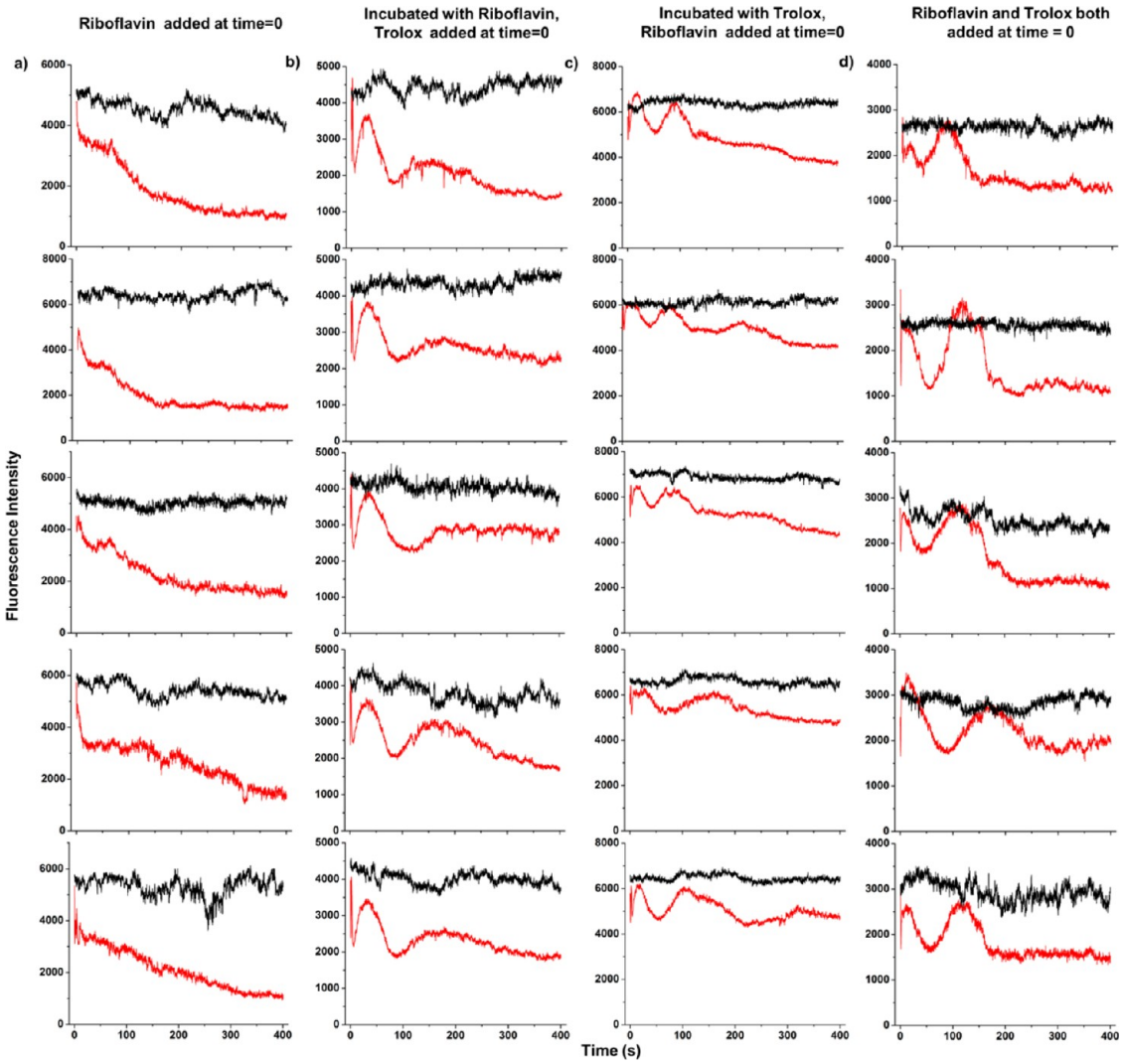

Figure 2. Representative fluorescence intensity−time traces (red) of individual SWCNTs in the presence of oxygen for five nanotubes after being exposed to (a) just riboflavin addition, (b) Trolox addition after riboflavin incubation, (c) riboflavin addition after Trolox incubation, and (d) riboflavin and Trolox addition at the same time for a final concentration of 1 mM for Trolox and 100 μM for riboflavin. Corresponding control traces in the absence of analyte addition (black) are shown for comparison.

SWCNT films were recorded. A sample image collected by the microscope is shown in Figure 1g. In the analysis, nanotubes were located based on the first frame of the movie. Therefore, it is essential that the nanotubes remain stationary throughout the course of the movie. Since the diffraction-limited spots of individually fluorescent nanotubes result in 2 × 2 pixelated bright spots,[32] the intensities in the first image of the movie were averaged over 2 × 2 pixelated regions, and the brightest pixelated regions corresponding to individual SWCNTs were selected. Spectral measurements of the pixelated regions performed in previous studies[51] verify individual SWCNT emissions. The fluorescence from the nanotubes located near the outer boundary of the illumination spot is susceptible to laser-induced fluctuations in intensity. To avoid this, the image was cropped to select only a region of interest (ROI) that excluded boundary SWCNTs (Figure 1h). The 200 brightest 2 × 2 pixelated regions were subsequently selected from the pixels located within this ROI (Figure 1i). Representative intensity−time traces for selected individual SWCNTs (circled as X, Y, Z in Figure 1i) in the presence of oxygen for Trolox addition after riboflavin incubation is provided in Figure 1j. Fluorescence intensity−time traces (red) of an individual SWCNT in the presence of oxygen for the first five brightest nanotubes after exposure to (b) just riboflavin, (c) Trolox addition after riboflavin incubation, (d) riboflavin addition after Trolox incubation, and (e) riboflavin and Trolox addition simultaneously are shown in Figure 2. When riboflavin is added to the solution, a gradual quenching in the nanotube intensity was observed, whereas in the presence of both riboflavin and Trolox, an oscillatory quenching behavior was observed. On the other hand, control traces in the absence of additives (Figure 2, black) have

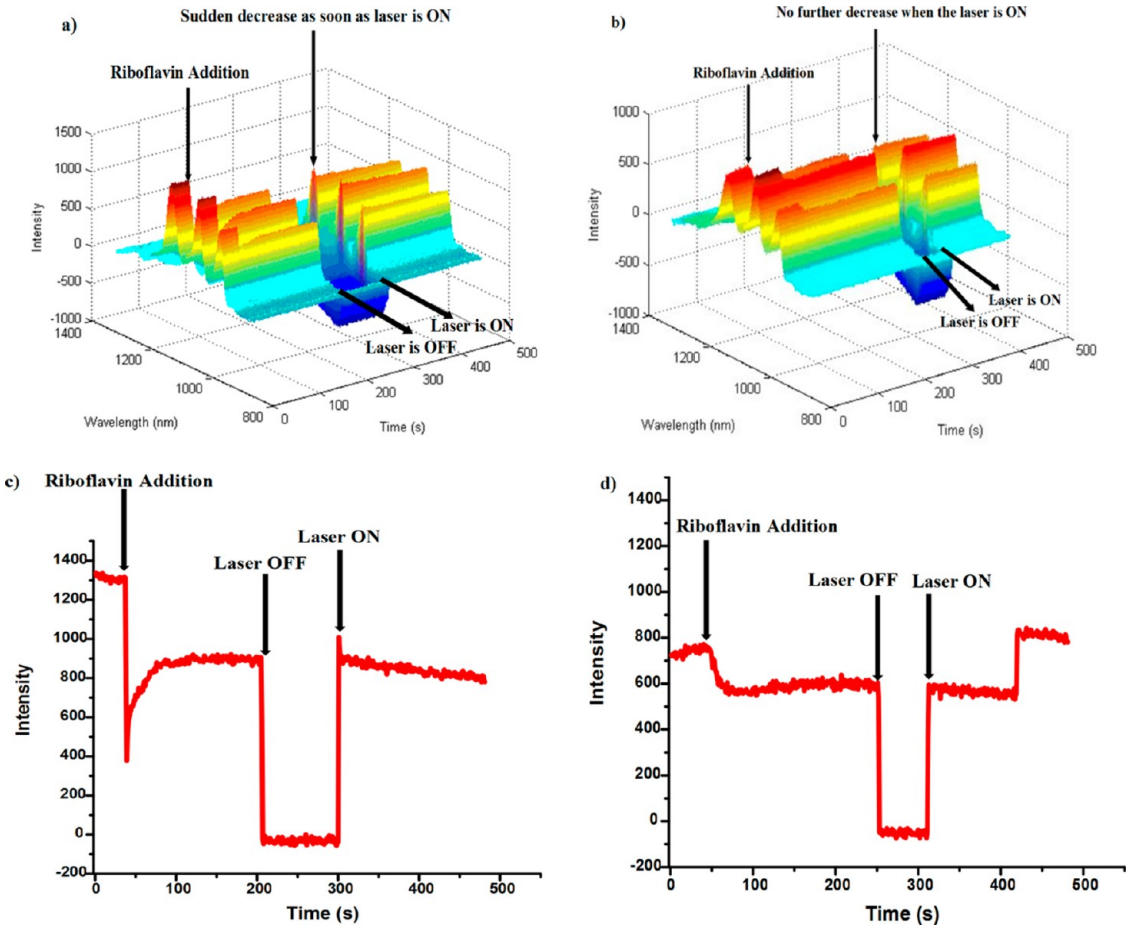

Figure 3. 3-D image showing laser effect on SWCNT response with the addition of riboflavin (a) in the presence of oxygen and (b) in the absence of oxygen. Cross sectional plot for the (7,6) nanotube chirality (c) in the presence of oxygen and (d) in the absence of oxygen.

relatively stable baselines compared to the decreasing and oscillatory traces in the presence of analyte. The fluctuations in such baseline intensities, which can be attributed to local variation in pH, concentration, dielectric, and other factors affecting SWCNT emission, have calculated rate constants that are an order of magnitude below those achieved in the presence of analyte.[31]

As discussed in previous studies, riboflavin illumination results in singlet oxygen and radical oxygen generation,[20−22] both of which act as quenchers of SWCNT fluorescence. The 3-D spectrum shown in Figure 3a shows the effect of photogenerated ROS on a range of SWCNT emission wavelengths from a variety of SWCNT chiralities. Riboflavin addition resulted in the immediate, uniform quenching of intensities across all nanotube chiralities. When the laser was turned off for approximately 2 min and then subsequently turned on again, intensity recovery over 2 frames was initially observed, followed by a sudden quenching. These observations indicate that the primary source of ROS quenching is photogeneration of singlet oxygen that is produced upon riboflavin illumination. A cross-sectional view of the 3-D plot at a single fluorescence wavelength for the (7,6) nanotube chirality (Figure 3c) elucidates this effect.

The observed singlet oxygen effect on SWCNT quenching was hypothesized to contribute to the oscillatory quenching behavior observed in Figures 2b−2d. To test this, all cases were repeated in the absence of oxygen. Figure 4 represents the corresponding fluorescence intensity−time traces (red) of an individual SWCNT in the absence of oxygen for first five brightest nanotubes after being exposed to (a) just riboflavin addition, (b) Trolox addition after riboflavin incubation, and (c) riboflavin addition after Trolox incubation. Corresponding changes in intensity distributions in the absence of oxygen are shown in Figure 5.

As shown in Figures 4a and 5a, riboflavin addition alone has no significant effect on SWCNT quenching in the absence of oxygen. Only in the presence of Trolox, a non-photosensitive compound, is quenching behavior observed, which is attributed to a decrease in Trolox concentration due to Trolox−riboflavin complexation. The 3-D plot given in Figure 3b and corresponding cross-section in Figure 3d further illustrate that in the absence of oxygen, no quenching is observed across several nanotube wavelength emissions.

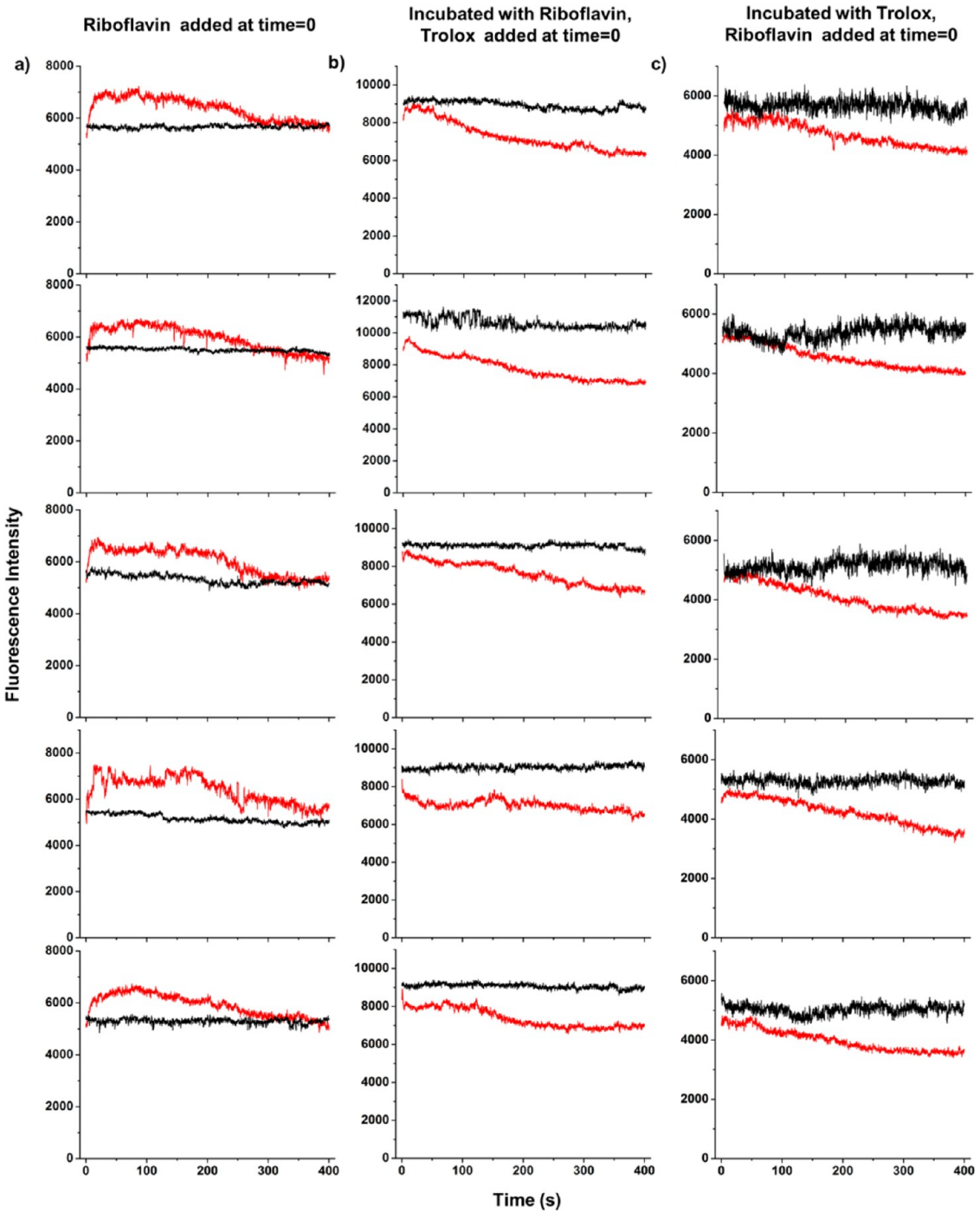

Figure 4. Representative fluorescence intensity–time traces (red) of an individual SWCNT in the absence of oxygen after being exposed to (a) just riboflavin addition, (b) Trolox addition after riboflavin incubation, and (c) riboflavin addition after Trolox incubation. Corresponding control traces in the absence of analyte addition (black) are shown for comparison.

Moreover, as shown in Figure 4, no oscillatory quenching behavior is observed in the absence of oxygen, indicating that the oscillation only occurs in the presence of oxygen and is hence attributed to ROS production. In the presence of Trolox (Figures 4b,c), very little quenching was observed in the absence of oxygen, which may be due to the decrease in Trolox concentration over time.

To elucidate the mechanism behind the observed oscillatory behavior, the photochemical Trolox–riboflavin reaction pathway was modeled (Figure 6). In our previous studies,[56] a Markov model was used to derive concentration-dependent rate constants for nonreactive systems using the intensity *versus* time traces. Such traces displayed step-like changes in intensity with discretized transitions used to quantify stochastic binding and unbinding instances. The intensity traces obtained from this reactive system, on the other hand, lack such discretized changes in intensity and thus

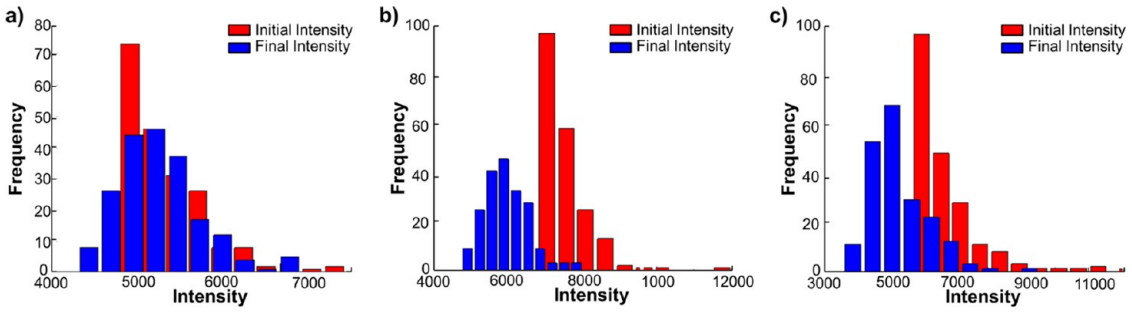

Figure 5. Histograms showing frequency distributions of starting and ending intensities for (a) just riboflavin addition, (b) Trolox addition after riboflavin incubation, and (c) riboflavin addition after Trolox incubation in the absence of oxygen.

cannot be quantified using the Markov model. The model presented in Figure 6 is based on an adaptation of the Trolox−riboflavin reaction system described by Gutièrrez and co-workers in methanol (where complexation between riboflavin and Trolox under aqueous conditions is avoided).[21] Initiation occurs with the photoexcitation of riboflavin from the ground state to the singlet state, as shown in reaction R1.

$$\mathrm{Rf} \xrightarrow[h\nu]{k_1} {}^1\mathrm{Rf}^* \qquad \textbf{(R1)}$$

The instability of singlet riboflavin results in the spontaneous relaxation of riboflavin to the triplet state. Triplet-state riboflavin may either relax to the ground state according to reaction R2 or further interact with other reactants in the solution (reactions R3−R5).

$$^3\mathrm{Rf}^* \xrightarrow{k_2} \mathrm{Rf} \qquad \textbf{(R2)}$$

Photoexcitation of riboflavin into the singlet and triplet states has been quantified in previous studies using laser flash photolysis[57−60] and double-pulse fluorescence.[61] Photoabsorption allows for several possible state transitions, depending on the nature of the excitation source. For instance, ground-state (S_0) absorption may result in excitation to the first level (S_1) or a higher level (S_n) singlet energy state. Similarly, excitation transitions are also possible from lower energy singlet to higher energy singlet states ($S_1 \rightarrow S_n$), as well as from lower energy to higher energy triplet states ($T_1 \rightarrow T_n$). At high excitation energies, singlet excited-state absorption is possible. However, at intensities below 10^9 W/cm^2, ground-state absorption is mostly observed. With typical excitation rates ranging between 10^{13} and 10^{15} s^{-1}, an excitation rate constant of 10^{13} s^{-1} was assumed.

Under continuous illumination, the system approaches steady-state concentrations as excited states simultaneously undergo several relaxation transitions. For instance, singlet riboflavin may undergo fluorescence (F) or internal conversion (IC) to the ground state ($S_1 \rightarrow S_0$) or intersystem conversion (ISC) to the triplet state ($S_1 - T_1$), with quantum efficiencies of $\Phi_F = 0.267$, $\Phi_{IC} = 0.36$, and $\Phi_{ISC} = 0.375$. In an analogous manner, the system may also undergo phosphorescence from the triplet to the ground state ($T_1 \rightarrow S_0$). As is the case with absorption, relaxation transitions are also possible among excited energy states ($S_n \rightarrow S_1$, $T_n \rightarrow T_1$), though on a much smaller time scale ($\tau \approx 1-100$ fs) than that of phosphorescence, fluorescence, and intersystem transitioning ($\tau \approx 1-1000$ μs), allowing one to assume spontaneous higher energy state transitions on the reactive time scale.[2] Provided the unstable nature of the singlet state, which ultimately relaxes to the ground and triplet states, singlet-state concentrations are typically low (~ 0 mM). In this study, singlet concentrations are considered to be negligible as relaxation to the triplet state is assumed to occur spontaneously over this reaction time scale.

In the triplet state, riboflavin may undergo type-I or type-II reaction mechanisms with either Trolox (reactions R3 and R4) or ground-state oxygen ($O_2(^3\Sigma_g)^-$) (reaction R5), as shown below.

$$^3\mathrm{Rf}^* + \mathrm{Tx} \xrightarrow{k_3} \mathrm{Rf} + \mathrm{Tx} \qquad \textbf{(R3)}$$

$$^3\mathrm{Rf}^* + \mathrm{Tx} \xrightarrow{k_4} \mathrm{Rf}^{\bullet -} + \mathrm{Tx}^{\bullet +} \qquad \textbf{(R4)}$$

$$^3\mathrm{Rf}^* + \mathrm{O_2}(^3\Sigma_g)^- \xrightarrow{k_5} \mathrm{Rf} + \mathrm{O_2}(^1\Delta_g) \qquad \textbf{(R5)}$$

In the presence of excess Trolox (≥30 mM), the photodecomposition of riboflavin is prevented through excessive quenching of the singlet state. However, modest Trolox concentrations (<1 mM) such as those used in this study, allow for the photogeneration of triplet riboflavin. As shown in reaction R5, the quenching of riboflavin in the triplet state forms singlet oxygen ($O_2(^1\Delta_g)$), which, together with superoxide ($O_2^{\bullet -}$), contributes to the irreversible degradation of both Trolox and riboflavin. For instance, the reaction of Trolox with superoxide yields an unstable intermediate, TxO*, which quickly relaxes to TxO according to the reaction

$$\mathrm{Tx} + \mathrm{O_2^{\bullet -}} \xrightarrow{k_6} \mathrm{TxO}^* \rightarrow \mathrm{TxO} \qquad \textbf{(R6)}$$

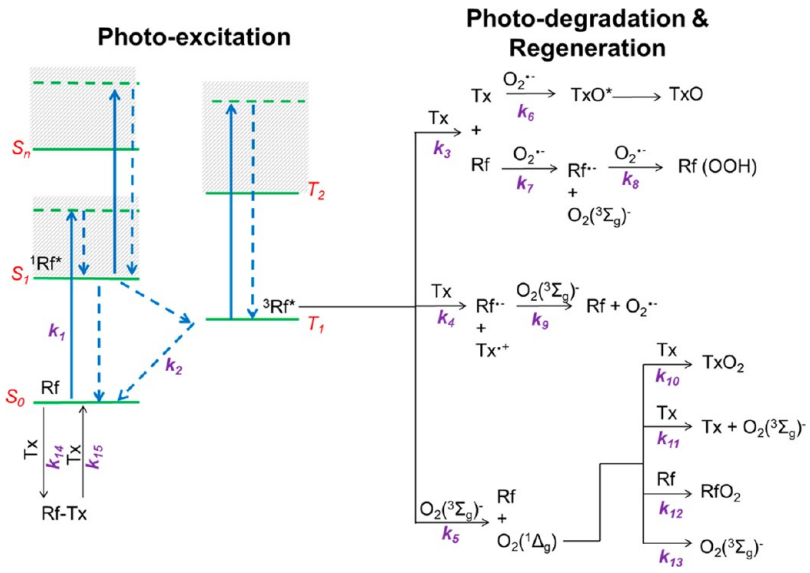

Figure 6. Reaction system for riboflavin and Trolox interactions. The schematic diagram summarizes the mechanism behind ground-state Rf photoexcitation (left) and ROS generation (right). Photoexcitation of Rf with a rate constant of k_1 results in the formation of singlet excited-state ^{1}Rf*, which subsequently relaxes down to the triplet state ^{3}Rf*. The ^{3}Rf* can either relax to the ground state with a rate constant of k_2, or it can react with Tx or ground-state $O_2(^3\Sigma_g)^-$. In one reaction with Tx (top, right), ^{3}Rf* relaxes with a rate constant of k_3 to form ground-state Tx and Rf. The Tx and Rf can each react with $O_2\cdot^-$ with rate constants of k_6 and k_7, respectively. In the first reaction, Tx forms a reactive oxide, TxO*, which immediately relaxes to the ground state, TxO. In the second reaction, Rf forms a reactive radical, Rf·⁻, which further reacts with $O_2\cdot^-$ with a rate constant of k_8 to form Rf(OOH). In an alternative pathway, ^{3}Rf* may react with Tx with a rate constant of k_4 to directly form Rf·⁻ and the Trolox radical Tx·⁺. The Rf·⁻ can further react with $O_2(^3\Sigma_g)^-$ to regenerate Rf and create $O_2\cdot^-$ with a rate constant of k_9. In a competing pathway, ^{3}Rf* may alternatively react with $O_2(^3\Sigma_g)^-$ to form Rf and $O_2(^1\Delta_g)$ with a rate constant of k_5. The reactive $O_2(^1\Delta_g)$ can react with Tx with a rate constant of k_{10} and k_{11} to formTxO_2 or regenerate $O_2(^3\Sigma_g)^-$, respectively. The $O_2(^1\Delta_g)$ can also react with Rf with a constant of k_{12} to form RfO_2 or with a constant of k_{13} to regenerate $O_2(^3\Sigma_g)^-$. In this reaction scheme, $O_2(^1\Delta_g)$ and $O_2\cdot^-$ decrease SWCNT fluorescence and Tx increases SWCNT fluorescence. The corresponding rate constant for each reaction is designated k_{1-15} (purple). The singlet-state energy levels for riboflavin are noted as S_{0-n}, and the triplet-state energy levels are noted as T_{1-2} (red). Energy levels are not drawn to scale. Legend: riboflavin (Rf), singlet excited-state riboflavin (^{1}Rf*), triplet excited-state riboflavin (^{3}Rf*), riboflavin radical anion (Rf·⁻), riboflavin dioxide (RfO_2), riboflavin peroxide (RfOOH), Trolox (Tx), Trolox radical cation (Tx·⁺), Trolox oxide (TxO), excited state Trolox oxide (TxO*), Trolox dioxide (TxO_2), ground-state oxygen ($O_2(^3\Sigma_g)^-$), singlet excited state oxygen ($O_2(^1\Delta_g)$), superoxide ($O_2\cdot^-$).

Riboflavin may also react with superoxide to yield a riboflavin radical (reaction R7) that can further react with superoxide to form a peroxide (reaction R8).

$$Rf + O_2^{\bullet -} \xrightarrow{k_7} Rf^{\bullet -} + O_2(^3\Sigma_g)^- \quad \textbf{(R7)}$$

$$Rf^{\bullet -} + O_2^{\bullet -} \xrightarrow{k_8} Rf(OOH) \quad \textbf{(R8)}$$

In addition to superoxide, the riboflavin radical can also react with ground-state oxygen (reaction R9) to generate the superoxide reactant used in reactions R6–R8.

$$Rf^{\bullet -} + O_2(^3\Sigma_g)^- \xrightarrow{k_9} Rf + O_2^{\bullet -} \quad \textbf{(R9)}$$

Singlet oxygen formed from reaction R5 may also further react with Trolox (reactions R10 and R11) and riboflavin (reaction R12) to irreversibly generate oxides, according to the reaction shown below.

$$Tx + O_2(^1\Delta_g) \xrightarrow{k_{10}} TxO_2 \quad \textbf{(R10)}$$

$$Tx + O_2(^1\Delta_g) \xrightarrow{k_{11}} Tx + O_2(^3\Sigma_g)^- \quad \textbf{(R11)}$$

$$Rf + O_2(^1\Delta_g) \xrightarrow{k_{12}} RfO_2 \quad \textbf{(R12)}$$

The excited-state oxygen may also spontaneously relax to the ground state,

$$O_2(^1\Delta_g) \xrightarrow{k_{13}} O_2(^3\Sigma_g)^- \quad \textbf{(R13)}$$

Under aqueous conditions, riboflavin and Trolox undergo a reversible complexation reaction, which is also included in this model (reactions R14–R15).

$$Rf + Tx \xrightarrow{k_{14}} Rf - Tx \quad \textbf{(R14)}$$

$$Rf - Tx \xrightarrow{k_{15}} Rf + Tx \quad \textbf{(R15)}$$

A summary of the corresponding rate constants for this reaction network is presented in Table 1. As noted in the Table, values for the most part are derived directly from the literature. The rate constant for the riboflavin–Trolox association reaction was calculated assuming diffusion-controlled conditions according to the expression

$$k_{14} = 4\pi(r_{Rf} + r_{Tx})(D_{Rf} + D_{Tx}) \quad \textbf{(E1)}$$

where r_{Rf} and r_{Tx} are the riboflavin and Trolox molecular radii, and D_{Rf} and D_{Tx} are the corresponding diffusion coefficients for riboflavin and Trolox, respectively.

Using coefficient values of $D_{Rf} = 3.23 \times 10^{-10}$ m^2/s[58] and $D_{Tx} = 5 \times 10^{-10}$ m^2/s[59], the molecular radii can be calculated according to the Stokes–Einstein relation

$$r = \frac{k_B T}{6\pi\eta D} \quad \text{(E2)}$$

where k_B is the Boltzmann constant, T is temperature, and η is viscosity. With a calculated forward rate constant of $k_{14} = 7 \times 10^9$ M^{-1}s^{-1}, a reverse rate constant of $k_{15} = 9 \times 10^7$ s^{-1} was calculated by dividing the forward constant by the apparent association constant of 79 M^{-1}.[25]

TABLE 1. Literature Reaction Rate Constants for the Network in Figure 6 in Bulk Solution[a]

rate constant	value	rate constant	value
k_1	10^{13} s^{-1}	k_9[c]	1.4×10^8 M^{-1} s^{-1}
k_2[b]	3.7×10^4 s^{-1}	k_{10}[g]	2.2×10^8 M^{-1} s^{-1}
k_3[c]	4.7×10^9 M^{-1} s^{-1}	k_{11}[g]	1.3×10^8 M^{-1} s^{-1}
k_4[d]	6.2×10^8 M^{-1} s^{-1}	k_{12}[c]	6×10^7 M^{-1} s^{-1}
k_5[c]	9×10^8 M^{-1} s^{-1}	k_{13}[h]	5×10^5 s^{-1}
k_6[e]	1.7×10^4 M^{-1} s^{-1}	k_{14}[i]	7×10^9 M^{-1} s^{-1}
k_7[f]	10^6 M^{-1} s^{-1}	k_{15}[j]	9×10^8 s^{-1}
k_8[f]	8.5×10^8 M^{-1} s^{-1}		

[a] All rate constants, except k_{14}, were evaluated based on values determined in the literature. The rate constant k_{14} was approximated assuming diffusion-controlled conditions using diffusion coefficients derived from the literature. Appropriate citations are provided as follows. [b] Islam *et al.* (2003)[57] using double-pulse measurements in aqueous solution at pH 7; k_1 was calculated based on the combined radiative and internal conversion rates of $k_{rad} = 5.28 \times 10^7$ s^{-1} and $k_{IC} = 7.1 \times 10^7$ s^{-1}. k_3 is calculated from the phosphorescence time constant of $\tau_p = 27$ μs. [c] Gutièrrez *et al.* (2001)[25] in methanol. [d] Cardoso *et al.* (2007)[1]. [e] Nishikimi and Machlin (1975).[64] [f] Afanas'ev (1991)[65] for glucose oxidase reaction with superoxide anion. [g] Nonell *et al.* (2005).[66] k_{10} is based on the reported reactive rate constant $k_r = 2.2 \times 10^8$ M^{-1} s^{-1}, whereas k_{11}, the quenching rate constant (k_q), is calculated as the difference between the total rate of $k_t = 3.5 \times 10^8$ M^{-1} s^{-1} and k_r. [h] Wilkinson & Brummer (1981).[67] [i] Association rate constant was calculated assuming diffusion-controlled conditions. The Trolox diffusion coefficient was taken as 5×10^{-10} m^2/s from Masuhara *et al.* (2007),[59] and the riboflavin diffusion coefficient was taken as 3.23×10^{-10} m^2/s from de Jesus *et al.* (2012).[58] [j] Dissociation rate constant was calculated from the association rate constant k_{14} and the equilibrium rate constant of 79 M^{-1} from Gutièrrez *et al.* (2001)[25] using the Benessi–Hildebrandt method as described by Forster (1969).[68]

It is important to note that though the network of reactions is assumed to occur homogenously in solution, as shown in Figure 1b, the sensing mechanism is confined to the APTES-functionalized glass surface containing the nanotube-based sensors. As shown in Figure 7, the nanotube sensors are surrounded by hydrophobic, APTES molecular chains that hinder analyte access to the nanotube surface. To accurately model the detection of the reaction products by the sensors, this model introduces a partition coefficient, κ,

$$\kappa = \frac{[C]_{film}}{[C]_{bulk}} \quad \text{(E3)}$$

The partition coefficient, which is the ratio of the concentration of the analyte in the vicinity of the sensor film, $[C]_{film}$, to that in the bulk solution, $[C]_{bulk}$, accounts for the heterogeneity of the analyte concentration in the Petri dish. The value of this partition coefficient was determined by fitting the model to representative experimental traces. However, it should be noted that this involves only three adjustable parameters, maintaining that the reaction network and literature values for rate constants describe the complex, oscillatory response of the emission.

The starting concentrations for Trolox and riboflavin used in this model are 0.89 mM and 0.1 mM, respectively, with a dissolved oxygen concentration of 0.26 mM. With concentrations on the order of ~0.1 mM and second-order reaction rate constants $<10^9$ M^{-1} s^{-1}, as expected, the corresponding first-order reaction rates of $<10^5$ s^{-1} are significantly slower than the riboflavin state transitions ($>10^7$ s^{-1}), which may be assumed to spontaneously equilibrate wherein quantum efficiencies are essentially maintained throughout the reaction scheme.

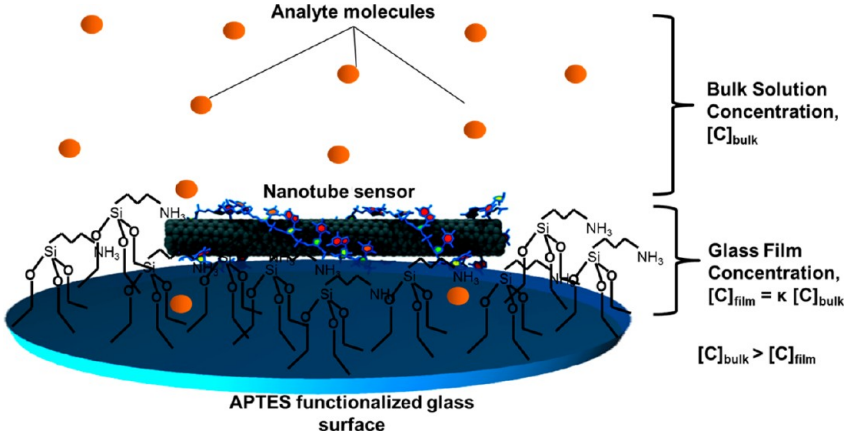

Figure 7. Role of partition coefficient in determining analyte concentration. The sensing mechanism relies on the interaction of the analyte (orange spheres) with the DNA-wrapped nanotube sensor, which is adsorbed onto an APTES functionalized glass surface. The partition coefficient provides the ratio of the concentration of the analyte in the APTES film atop the glass surface to that in the bulk phase.

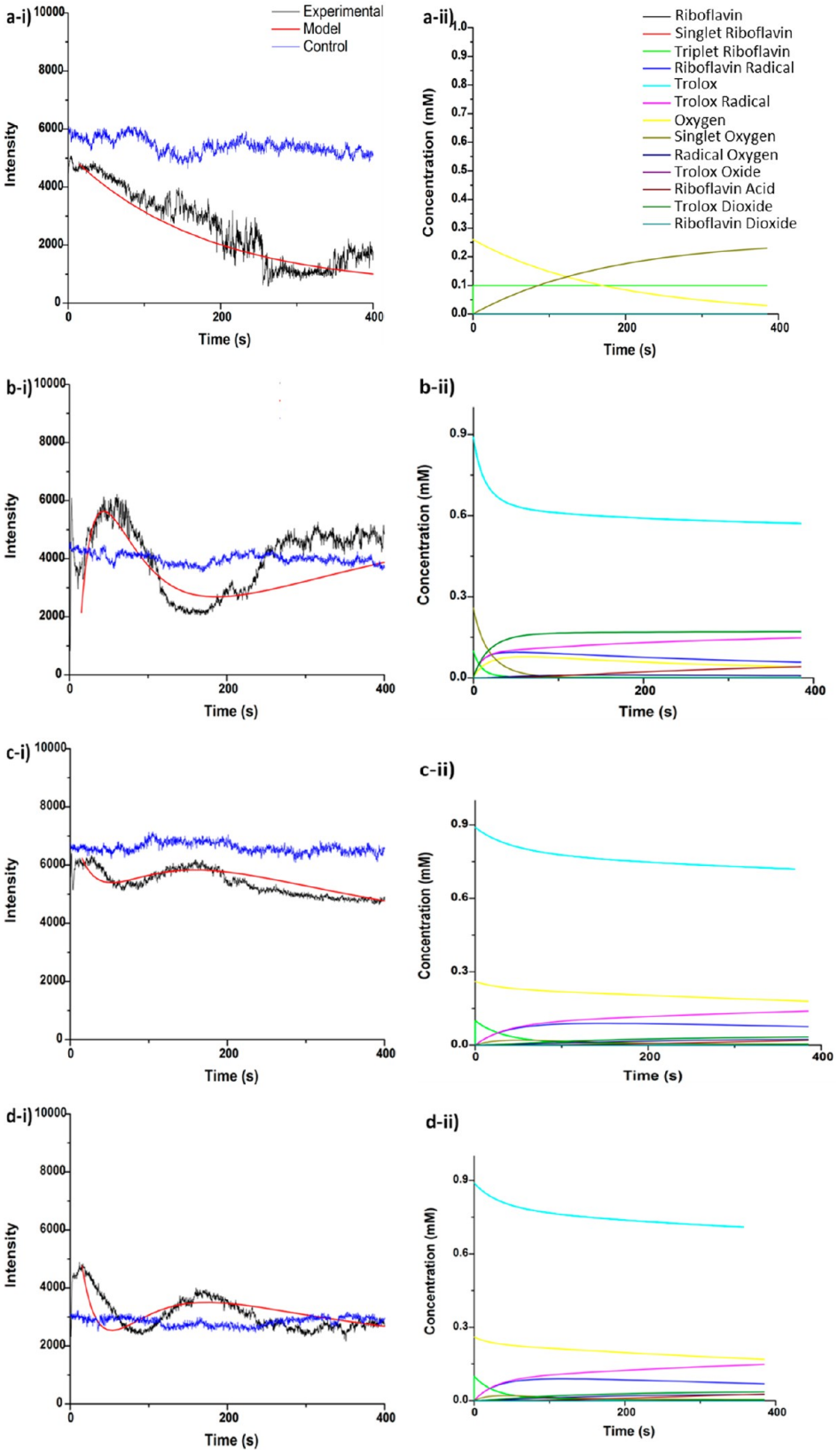

Figure 8. (i) Representative control trace (blue), experimental trace (black), and fitted model trace (red) of an individual SWCNT in the presence of oxygen. (ii) Normalized concentrations of the reactive products after being exposed to (a) just riboflavin addition, (b) Trolox addition after riboflavin incubation, (c) riboflavin addition after Trolox incubation, and (d) riboflavin and Trolox addition simultaneously.

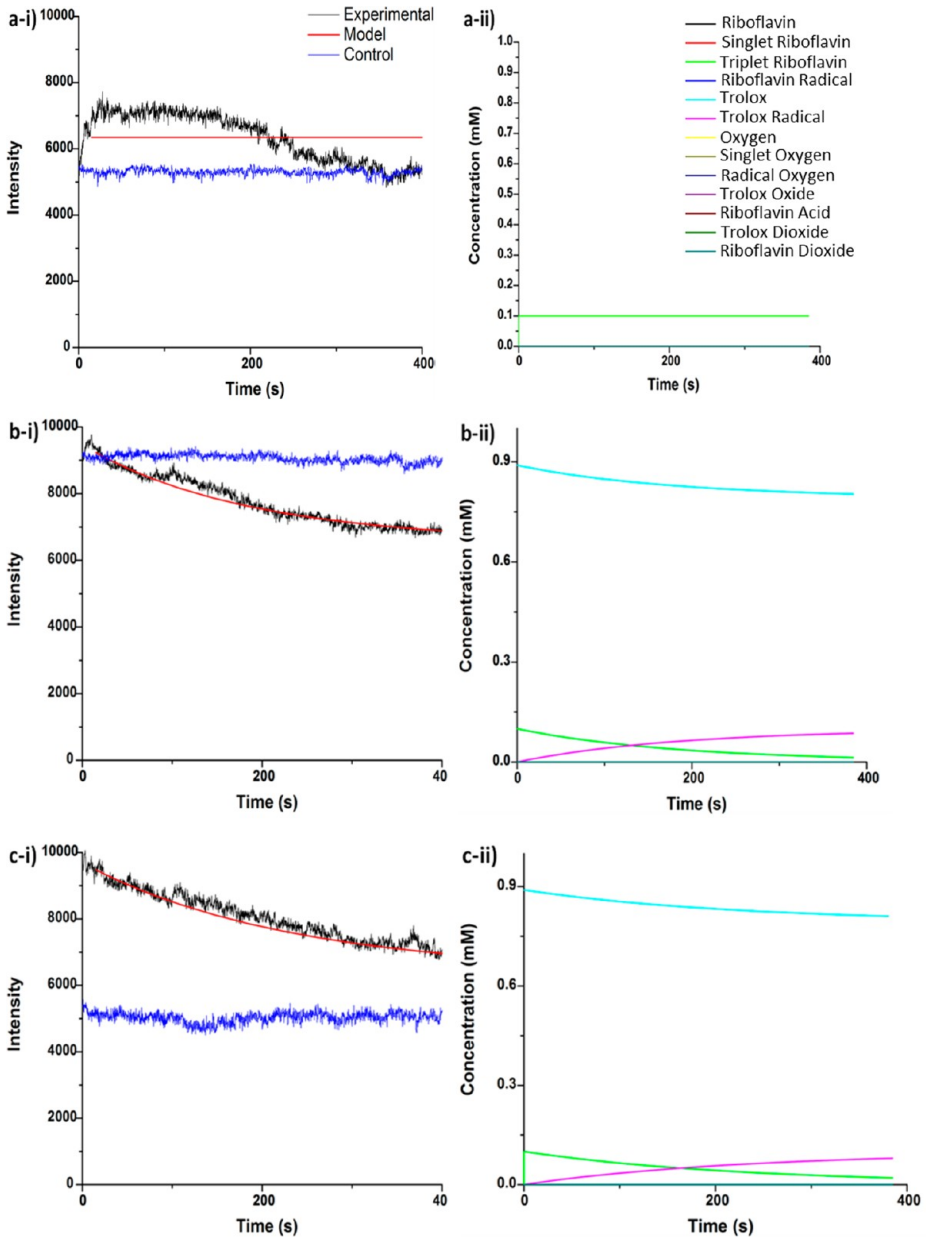

Figure 9. (i) Representative control trace (blue), experimental trace (black), and fitted model trace (red) of an individual SWCNT in the absence of oxygen. (ii) Normalized concentrations of the reactive products after being exposed to (a) just riboflavin addition, (b) Trolox addition after riboflavin incubation, and (c) riboflavin addition after Trolox incubation.

The predicted fluorescence oscillations are shown in Figure 8a–d(i), along with sample experimental and control traces. The best-fit partition coefficient for the traces used in this study ranged from 10^{-6}–10^{-4}. The resulting concentrations of the reactants and products over time based on these coefficient values are shown in Figure 8a–d(ii). As shown in the control experiments, Trolox modulates nanotube fluorescence even in the absence of oxygen. Riboflavin modulation, however, is more strongly dependent on the presence of oxygen, alluding to the fact that nanotube fluorescence is indirectly affected by riboflavin *via* the formation of ROS. To model the effects of the reactive products on nanotube fluorescence, we examined the sum of the normalized concentrations, adding products (Trolox) that are expected to increase nanotube fluorescence and subtracting those (singlet oxygen, radical oxygen) that are expected to decrease nanotube fluorescence (Figure 8a–d(i)). These plots demonstrate oscillations that are reminiscent of those seen in the experimental data with inflection points that coincide with those observed experimentally.

Similarly, we examined the predicted concentrations in the absence of oxygen (Figure 9). In the absence of oxygen, only the effects of the decreasing concentration of Trolox are seen, as singlet oxygen species are no longer generated by riboflavin. Again, the traces

shown in Figure 9a–d(i) are reminiscent of those seen experimentally in the absence of oxygen.

CONCLUSION

In this study, single-molecule detection of the photochemical reactions that occur in the presence of Trolox and riboflavin in both the presence and absence of oxygen was observed for the first time. Single-molecule oscillatory behavior was observed as binding analytes that enhance (Trolox) and quench (ROS) SWCNT fluorescence compete for binding sites on the SWCNT sensor. The series of photoelectrochemical reactions was modeled, and the modeling results were able to qualitatively predict the fluorescence behavior of the nanotube sensors.

METHODS AND MATERIALS

DNA Oligonucleotide Nanotube Suspension. SWCNTs were wrapped with $d(AT)_{15}$ oligonucleotide (Figure 1a) using a previously published method.[31,33] Briefly, HiPCO SWCNTs purchased from Unidym were suspended in 0.1 M NaCl with a 30-base (dAdT) sequence of ssDNA (Integrated DNA Technologies) in a 2:1 DNA:SWCNT mass ratio, with typical DNA concentrations of 2 mg/mL. After 10 min sonication with a 3 mm probe tip (Cole-parmer) at a power of 10 W, samples were centrifuged for 180 min with a benchtop centrifuge (Eppendorf Centrifuge 5415D) at 16 100 RCF. After centrifugation, the supernatant was collected and the pellet was discarded.

Trolox Solution. A 50 mM Trolox solution was made by dissolving 0.125 g of Trolox in 10 mL of methanol. Since Trolox is highly soluble in methanol, complete dissolution was obtained immediately upon mixing. In all experiments, appropriate amounts of Trolox solution were added to yield a final Trolox concentration of 1 mM. Since recent studies[33] have shown that the addition of a pure methanol solution in the absence of Trolox does not affect SWCNT fluorescence, the effects of solvent mixing is negligible for the volumes used in this study. Trolox was purchased from Sigma-Aldrich and stored in 2–8 °C.

Riboflavin Solution. A 0.37 mM riboflavin stock solution was prepared by dissolving 2.8 mg of riboflavin in 20 mL of water. In all experiments, appropriate amounts of riboflavin solution were added to yield a final concentration of 100 uM riboflavin. Riboflavin was purchased from Sigma-Aldrich and stored at room temperature.

Microscopy and Data Collection for Single Molecule Detection. DNA-SWCNT films were prepared according to previously published methods.[31,33] Briefly, a 200 μL droplet of APTES was added to the bottom of a glass-bottomed Petri dish (Mattek P35G-1.5-14-C) for surface pretreatment and subsequently rinsed 3 times with 1 × PBS. Then, 200 μL of the DNA oligonucleotide–SWCNT solution was added to the glass surface and incubated for 2–3 min. The SWCNT solution was then removed and the Petri dish was once more rinsed 3 times with buffer. The film was incubated for 5–10 min prior to the addition of 2 mL of PBS buffer. In the single-molecule microscope measurements, AT_{15}–SWCNT samples were excited by a 658 nm laser (LDM-OPT-A6-13, Newport Corp) at 33.8 mW and fluorescence emission was monitored in real time through a 100× TIRF objective using an inverted microscope (Carl Zeiss, Axiovert 200) with a 2D InGaAs array (Princeton Instruments OMA 2D). Movies were recorded using a WinSpec data acquisition program (Princeton Instruments) at 0.2 s/frame. Before each recording, a control movie, with the same movie length as the non-control movie, was taken to ensure a stable baseline. Stabilization was subsequently followed by riboflavin and/or Trolox injection. Measurements were recorded immediately upon analyte injection at time = 0. The final molar ratio of Trolox to riboflavin to SWCNT (assuming an average of 10^6 amu with the initial incubation volume of the SWCNT solution) added to the Petri dish was *ca.* 1 mM:0.1 mM:0.071 mM.

For experiments conducted in the absence of oxygen, 3 mL of PBS, Trolox, and riboflavin were introduced into 5 mL round-bottom flasks. The flasks were sealed with septums with two protruding needles to provide for a gas inlet and outlet. This system was purged with argon gas (Airgas) for 2 h to remove dissolved oxygen in the buffer. Then, Trolox and/or riboflavin were injected through a fine hole, minimizing air exposure and preventing oxygen dissolution.

Conflict of Interest: The authors declare no competing financial interest.

REFERENCES AND NOTES

1. Cardoso, D. R.; Olsen, K.; Skibsted, L. H. Mechanism of Deactivation of Triplet-Excited Riboflavin by Ascorbate, Carotenoids, and Tocopherols in Homogeneous and Heterogeneous Aqueous Food Model Systems. *J. Agric. Food Chem.* **2007**, *55*, 6285–6291.
2. Martin, C. B.; Tsao, M. L.; Hadad, C. M.; Platz, M. S. The Reaction of Triplet Flavin with Indole. A Study of the Cascade of Reactive Intermediates Using Density Functional Theory and Time Resolved Infrared Spectroscopy. *J. Am. Chem. Soc.* **2002**, *124*, 7226–7234.
3. Shaw, J. H. Effect of Nutritional Factors on Bones and Teeth. *Ann. N.Y. Acad. Sci.* **1955**, *60*, 733–762.
4. Budavari, S. *The Merck Index: An Encyclopedia of Chemicals, Drugs, and Biologicals*; 12th ed.; Merck: Whitehouse Station, NJ, 1996.
5. Szczesni., T; Karabin, L.; Szczepan., M; Wituch, K. Biosynthesis of Riboflavin by Ashbya-Gossypii. 1. Influence of Fats of Animal Origin on Riboflavin Production. *Acta Microbiol. Pol.* **1971**, *3*, 29.
6. Warkany, J.; Roth, C. B.; Wilson, J. G. Multiple Congenital Malformations—A Consideration of Etiologic Factors. *Pediatrics* **1948**, *1*, 462–471.
7. Romanoff, A. L.; Bauernfeind, J. C. Influence of Riboflavin-Deficiency in Eggs on Embryonic Development (Gallus Domesticus). *Anat. Rec.* **1942**, *82*, 11–23.
8. Beal, V. A.; Vanbuskirk, J. J. Riboflavin in Red Blood Cells in Relation to Dietary Intake of Children. *Am. J. Clin. Nutr.* **1960**, *8*, 841–845.
9. Ajayi, O. A.; George, B. O.; Ipadeola, T. Clinical-Trial of Riboflavin in Sickle-Cell Disease. *East Afr. Med. J.* **1993**, *70*, 418–421.
10. Edwards, A. M.; Silva, E.; Jofre, B.; Becker, M. I.; Deioannes, A. E. Visible-Light Effects on Tumoral Cells in a Culture-Medium Enriched with Tryptophan and Riboflavin. *J Photochem. Photobiol. B* **1994**, *24*, 179–186.
11. Jung, M. Y.; Min, D. B. ESR Study of the Singlet Oxygen Quenching and Protective Activity of Trolox on the Photodecomposition of Riboflavin and Lumiflavin in Aqueous Buffer Solutions. *J. Food Sci* **2009**, *74*, C449–C455.
12. Jung, M. Y.; Yoon, S. H.; Lee, H. O.; Min, D. B. Singlet Oxygen and Ascorbic Acid Effects on Dimethyl Disulfide and Off-Flavor in Skim Milk Exposed to Light. *J. Food Sci.* **1998**, *63*, 408–412.
13. King, J. M.; Min, D. B. Riboflavin Photosensitized Singlet Oxygen Oxidation of Vitamin D. *J. Food Sci.* **1998**, *63*, 31–34.
14. Huang, R.; Choe, E.; Min, D. B. Effects of Riboflavin Photosensitized Oxidation on the Volatile Compounds of Soymilk. *J. Food Sci.* **2004**, *69*, C733–C738.
15. Kim, H.; Kirschenbaum, L. J.; Rosenthal, I.; Riesz, P. Photosensitized Formation of Ascorbate Radicals by Riboflavin—an ESR Study. *Photochem. Photobiol.* **1993**, *57*, 777–784.

16. Edwards, A. M.; Bueno, C.; Saldano, A.; Silva, E.; Kassab, K.; Polo, L.; Jori, G. Photochemical and Pharmacokinetic Properties of Selected Flavins. *J. Photochem. Photobiol. B* **1999**, *48*, 36–41.
17. Lee, S. W.; Chang, P. S.; Lee, J. H. Effects of Riboflavin Photosensitization on the Changes of Isoflavones in Soymilk. *J. Food Sci.* **2008**, *73*, C551–C555.
18. Yang, S.; Lee, S.; Chung, H.; Lee, J. Stability of Isoflavone Daidzein and Genistein in Riboflavin, Chlorophyll b, or Methylene Blue Photosensitization. *J. Food Sci.* **2008**, *73*, C100–C105.
19. Criado, S.; Castillo, C.; Yppolito, R.; Bertolotti, S.; Garcia, N. A. The Role of 4-and 5-Aminosalicylic Acids in a Riboflavin-Photosensitised Process. *J. Photochem. Photobiol. A* **2003**, *155*, 115–118.
20. Grzelak, A.; Rychlik, B.; Baptosz, G. Light-Dependent Generation of Reactive Oxygen Species in Cell Culture Media. *Free Radic. Biol. Med.* **2001**, *30*, 1418–1425.
21. Lucius, R.; Mentlein, R.; Sievers, J. Riboflavin-Mediated Axonal Degeneration of Postnatal Retinal Ganglion Cells *in Vitro* Is Related to the Formation of Free Radicals. *Free Radic. Biol. Med.* **1998**, *24*, 798–808.
22. Min, D. B.; Boff, J. M. Chemistry and Reaction of Singlet Oxygen in Foods. *Compr. Rev. Food Sci. Food Saf.* **2002**, *1*, 58–72.
23. Choe, E.; Huang, R.; Min, D. B. Chemical Reactions and Stability of Riboflavin in Foods. *J. Food Sci.* **2005**, *70*, R28–R36.
24. Ahmad, I.; Fasiliullah, Q.; Vaid, F. H. M. A Study of Simultaneous Photolysis and Photoaddition Reactions of Riboflavin in Aqueous Solution. *J Photochem. Photobiol. B* **2004**, *75*, 13–20.
25. Gutierrez, I.; Criado, S.; Bertolotti, S.; Garcia, N. A. Dark and Photoinduced Interactions Between Trolox, a Polar-Solvent-Soluble Model for Vitamin E, and Riboflavin. *J Photochem. Photobiol. B* **2001**, *62*, 133–139.
26. Huang, R.; Kim, H. J.; Min, D. B. Photosensitizing Effect of Riboflavin, Lumiflavin, and Lumichrome on the Generation of Volatiles in Soy Milk. *J. Agric. Food Chem.* **2006**, *54*, 2359–2364.
27. Kim, T. S.; Decker, E. A.; Lee, J. Antioxidant Capacities of α-Tocopherol, Trolox, Ascorbic Acid, and Ascorbyl Palmitate in Riboflavin Photosensitized Oil-in-Water Emulsions. *Food Chem.* **2012**, *133*, 68–75.
28. Hall, N. K.; Chapman, T. M.; Kim, H. J.; Min, D. B. Antioxidant Mechanisms of Trolox and Ascorbic Acid on the Oxidation of Riboflavin in Milk Under Light. *Food Chem.* **2010**, *118*, 534–539.
29. Jung, M. Y.; Choe, E.; Min, D. B. α-, γ- and δ-Tocopherol Effects on Chlorophyll Photosensitized Oxidation of Soybean Oil. *J. Food Sci.* **1991**, *56*, 807–810.
30. Boghossian, A. A.; Zhang, J. Q.; Barone, P. W.; Reuel, N. F.; Kim, J. H.; Heller, D. A.; Ahn, J. H.; Hilmer, A. J.; Rwei, A.; Arkalgud, J. R.; *et al*. Near-Infrared Fluorescent Sensors Based on Single-Walled Carbon Nanotubes for Life Sciences Applications. *Chemsuschem* **2011**, *4*, 848–863.
31. Zhang, J. Q.; Boghossian, A. A.; Barone, P. W.; Rwei, A.; Kim, J. H.; Lin, D. H.; Heller, D. A.; Hilmer, A. J.; Nair, N.; Reuel, N. F.; *et al*. Single Molecule Detection of Nitric Oxide Enabled by d(AT)(15) DNA Adsorbed to Near Infrared Fluorescent Single-Walled Carbon Nanotubes. *J. Am. Chem. Soc.* **2011**, *133*, 567–581.
32. Jin, H.; Heller, D. A.; Kim, J.-H.; Strano, M. S. Stochastic Analysis of Stepwise Fluorescence Quenching Reactions on Single-Walled Carbon Nanotubes: Single Molecule Sensors. *Nano Lett* **2008**, *8*, 4299–4304.
33. Sen, S.; Sen, F.; Boghossian, A. A.; Zhang, J. Q.; Strano, M. S. The Effect of Reductive Brightening Agents on the Sensitivity of SWCNT Fluorescent Sensors. *J. Phys. Chem. C* **2012**.
34. Bachilo, S. M.; Strano, M. S.; Kittrell, C.; Hauge, R. H.; Smalley, R. E.; Weisman, R. B. Structure-Assigned Optical Spectra of Single-Walled Carbon Nanotubes. *Science* **2002**, *298*, 2361–2366.
35. Hartschuh, A.; Pedrosa, H. N.; Novotny, L.; Krauss, T. D. Simultaneous Fluorescence and Raman Scattering from Single Carbon Nanotubes. *Science* **2003**, *301*, 1354–1356.
36. Dresselhaus, M. S.; Dresselhaus, G.; Eklund, P. C. *Science of Fullerenes and Carbon Nanotubes*; Academic Press: San Diego, 1996.
37. Cognet, L.; *et al*. Stepwise Quenching of Exciton Fluorescence in Carbon Nanotubes by Single-molecule Reactions. *Science* **2007**, *316*, 1465–1468.
38. Jin, H.; Heller, D. A.; Kim, J. H.; Strano, M. S. Stochastic Analysis of Stepwise Fluorescence Quenching Reactions on Single-Walled Carbon Nanotubes: Single Molecule Sensors. *Nano Lett.* **2008**, *8*, 4299–4304.
39. Jin, H.; *et al*. Detection of Single-molecule H_2O_2 Signalling from Epidermal Growth Factor Receptor Using Fluorescent Single-walled Carbon Nanotubes. *Nat. Nanotechnol.* **2010**, *5*, 302–309.
40. Zhang, J.; *et al*. Single Molecule Detection of Nitric Oxide Enabled by $d(AT)_{15}$ DNA Adsorbed to Near Infrared Fluorescent Single-Walled Carbon Nanotubes. *J. Am. Chem. Soc.* **2010**, *133*, 567–581.
41. O'Connell, M. J.; Boul, P.; Ericson, L. M.; Huffman, C.; Wang, Y. H.; Haroz, E.; Kuper, C.; Tour, J.; Ausman, K. D.; Smalley, R. E. Reversible Water-Solubilization of Single-Walled Carbon Nanotubes by Polymer Wrapping. *Chem. Phys. Lett.* **2001**, *342*, 265–271.
42. Islam, M. F.; Rojas, E.; Bergey, D. M.; Johnson, A. T.; Yodh, A. G. High Weight Fraction Surfactant Solubilization of Single-Wall Carbon Nanotubes in Water. *Nano Lett* **2003**, *3*, 269–273.
43. Haggenmueller, R.; Rahatekar, S. S.; Fagan, J. A.; Chun, J. H.; Becker, M. L.; Naik, R. R.; Krauss, T.; Carlson, L.; Kadla, J. F.; Trulove, P. C. Comparison of the Quality of Aqueous Dispersions of Single Wall Carbon Nanotubes Using Surfactants and Biomolecules. *Langmuir* **2008**, *24*, 5070–5078.
44. Yoon, H.; Ahn, J. H.; Barone, P. W.; Yum, K.; Sharma, R.; Boghossian, A. A.; Han, J. H.; Strano, M. S. Periplasmic Binding Proteins as Optical Modulators of Single-Walled Carbon Nanotube Fluorescence: Amplifying a Nanoscale Actuator. *Angew. Chem. Int. Ed.* **2011**, *50*, 1828–1831.
45. Barone, P. W.; Baik, S.; Heller, D. A.; Strano, M. S. Near-Infrared Optical Sensors Based on Single-Walled Carbon Nanotubes. *Nat. Mater.* **2005**, *4*, 86–U16.
46. Barone, P. W.; Strano, M. S. Reversible Control of Carbon Nanotube Aggregation for a Glucose Affinity Sensor. *Angew. Chem. Int. Ed.* **2006**, *45*, 8138–8141.
47. Jeng, E. S.; Moll, A. E.; Roy, A. C.; Gastala, J. B.; Strano, M. S. Detection of DNA Hybridization Using the Near-Infrared Band-Gap Fluorescence of Single-Walled Carbon Nanotubes. *Nano Lett.* **2006**, *6*, 371–375.
48. Heller, D. A.; Jeng, E. S.; Yeung, T. K.; Martinez, B. M.; Moll, A. E.; Gastala, J. B.; Strano, M. S. Optical Detection of DNA Conformational Polymorphism on Single-Walled Carbon Nanotubes. *Science* **2006**, *311*, 508–511.
49. Kim, J. H.; Ahn, J. H.; Barone, P. W.; Jin, H.; Zhang, J. Q.; Heller, D. A.; Strano, M. S. A Luciferase/Single-Walled Carbon Nanotube Conjugate for Near-Infrared Fluorescent Detection of Cellular ATP. *Angew. Chem. Int. Ed.* **2010**, *49*, 1456–1459.
50. Kim, J. H.; Heller, D. A.; Jin, H.; Barone, P. W.; Song, C.; Zhang, J.; Trudel, L. J.; Wogan, G. N.; Tannenbaum, S. R.; Strano, M. S. The Rational Design of Nitric Oxide Selectivity in Single-Walled Carbon Nanotube Near-Infrared Fluorescence Sensors for Biological Detection. *Nat. Chem.* **2009**, *1*, 473–481.
51. Cognet, L.; Tsyboulski, D. A.; Rocha, J. D. R.; Doyle, C. D.; Tour, J. M.; Weisman, R. B. Stepwise Quenching of Exciton Fluorescence in Carbon Nanotubes by Single-Molecule Reactions. *Science* **2007**, *316*, 1465–1468.
52. Lee, A. J.; Wang, X.; Carlson, L. J.; Smyder, J. A.; Loesch, B.; Tu, X.; Zheng, M.; Krauss, T. D. Bright Fluorescence from Individual Single-Walled Carbon Nanotubes. *Nano Lett.* **2011**, *11*, 1636–1640.
53. Heller, D. A.; Jin, H.; Martinez, B. M.; Patel, D.; Miller, B. M.; Yeung, T.-K.; Jena, P. V.; Hobartner, C.; Ha, T.; Silverman, S. K. Multimodal Optical Sensing and Analyte Specificity Using Single-Walled Carbon Nanotubes. *Nat. Nanotchnol.* **2009**, *4*, 114–120.

54. Boghossian, A. A.; Zhang, J. Q.; Le Floch-Yin, F. T.; Ulissi, Z. W.; Bojo, P.; Han, J. H.; Kim, J. H.; Arkalgud, J. R.; Reuel, N. F.; Braatz, R. D. The Chemical Dynamics of Nanosensors Capable of Single-Molecule Detection. *J. Chem. Phys.* **2011**, 135.
55. Ulissi, Z. W.; Zhang, J. Q.; Boghossian, A. A.; Reuel, N. F.; Shimizu, S. F. E.; Braatz, R. D.; Strano, M. S. Applicability of Birth−Death Markov Modeling for Single-Molecule Counting Using Single-Walled Carbon Nanotube Fluorescent Sensor Arrays. *J. Phys. Chem. Lett.* **2011**, *2*, 1690–1694.
56. Boghossian, A. A.; Zhang, J. Q.; Le Floch-Yin, F. T.; Ulissi, Z. W.; Bojo, P.; Han, J. H.; Kim, J. H.; Arkalgud, J. R.; Reuel, N. F.; Braatz, R. D.; *et al*. The Chemical Dynamics of Nanosensors Capable of Single-Molecule Detection. *J. Chem. Phys.* **2011**, 135.
57. Melo, T. B.; Ionescu, M. A.; Haggquist, G. W.; Naqvi, K. R. Hydrogen Abstraction by Triplet Flavins. I: Time-Resolved Multi-channel Absorption Spectra of Flash-Irradiated Riboflavin Solutions in Water. *Spectrochim Acta A* **1999**, *55*, 2299–2307.
58. Grodowski, M. S.; Veyret, B.; Weiss, K. Photochemistry of Flavins. 2. Photophysical Properties of Alloxazines and Isoalloxazines. *Photochem. Photobiol.* **1977**, *26*, 341–352.
59. Chacon, J. N.; Mclearie, J.; Sinclair, R. S. Singlet Oxygen Yields and Radical Contributions in the Dye-Sensitized Photo-oxidation in Methanol of Esters of Poly-Unsaturated Fatty-Acids (Oleic, Linoleic, Linolenic and Arachidonic). *Photochem. Photobiol.* **1988**, *47*, 647–656.
60. Krishna, C. M.; Uppuluri, S.; Riesz, P.; Zigler, J. S.; Balasubramanian, D. A Study of the Photodynamic Efficiencies of Some Eye Lens Constituents. *Photochem. Photobiol.* **1991**, *54*, 51–58.
61. Islam, S. D. M.; Penzkofer, A.; Hegemann, P. Quantum Yield of Triplet Formation of Riboflavin in Aqueous Solution and of Flavin Mononucleotide Bound to the LOV1 Domain of Phot1 from *Chlamydomonas Reinhardtii*. *Chem. Phys.* **2003**, *293*, 397–397.
62. de Jesus, M. B.; Fraceto, L. F.; Martini, M. F.; Pickholz, M.; Ferreira, C. V.; de Paula, E. Non-Inclusion Complexes between Riboflavin and Cyclodextrins. *J. Pharm. Pharmacol.* **2012**, *64*, 832–842.
63. Masuhara, H.; Kawata, S.; Tokunaga, F. *Nano Biophotonics: Science and Technology*, 1st ed.; Elsevier: Amsterdam; Boston, 2007.
64. Nichikimi, M.; Machlin, L. J. Oxidation of alpha-tocopherol model compound by superoxide anion. *Biochemistry and Biophysics* **1975**, *170* (2), 684–689.
65. Afanas'ev, I. B. Superoxide Ion Chemistry and Biological Implications. CRC Press: Boca Raton, FL, 1991; Vol. 2.
66. Nonell, S.; Moncayo, L.; Trull, F.; Amat-Guerri, F.; Lissi, E. A.; Soltermann, A. T.; Criado, S.; García, N. A. Solvent Influence on the Kinetics of the Photodynamic Degradation of Trolox, a Water Soluble Model Compound for Vitamin E. *J. Photochem. Photobiol. B: Biology* **1995**, *29*, 157–162.
67. Wilkinson, F.; Brummer, L. G. Rate Constants for the Decay and Reactions of the Lowest Electronically Excited Singlet State of Molecular Oxygen in Solution. *J. Phys. Chem. Ref. Data* **1981**, *10* (4), 809–1000.
68. Forster, R. Organic Charge Transfer Complexes Academic Press: New York, 1969.